Electronic damping of anharmonic adsorbate vibrations at metallic surfaces

Jean Christophe Tremblay,* Serge Monturet, and Peter Saalfrank
Institut für Chemie, Universität Potsdam, Karl-Liebknecht-Straße 24-25, D-14476 Potsdam-Golm, Germany
(Received 20 November 2009; revised manuscript received 22 January 2010; published 5 March 2010)

The nonadiabatic coupling of an adsorbate close to a metallic surface leads to electronic damping of adsorbate vibrations and line broadening in vibrational spectroscopy. Here, a perturbative treatment of the electronic contribution to the lifetime broadening serves as a building block for a new approach, in which anharmonic vibrational transition rates are calculated from a position-dependent coupling function. Different models for the coupling function will be tested, all related to embedding theory. The first two are models based on a scattering approach with (i) a jellium-type and (ii) a density functional theory based embedding density, respectively. In a third variant a further refined model is used for the embedding density, and a semiempirical approach is taken in which a scaling factor is chosen to match harmonic, single-site, first-principles transition rates, obtained from periodic density functional theory. For the example of hydrogen atoms on (adsorption) and below (subsurface absorption) a Pd(111) surface, lifetimes of and transition rates between vibrational levels are computed. The transition rates emerging from different models serve as input for the selective subsurface adsorption of hydrogen in palladium starting from an adsorption site, by using sequences of infrared laser pulses in a laser distillation scheme.

DOI: 10.1103/PhysRevB.81.125408 PACS number(s): 68.43.Pq, 82.53.St, 02.30.Yy, 32.80.Qk

I. INTRODUCTION

Energy relaxation is an ubiquitous problem when dealing with molecular dynamics in dissipative environments.[1–7] For example, for a vibrating molecule embedded in a "bath," the system vibrational states have finite lifetimes, which can affect their properties and chemical reactivity. Various relaxation channels can be operative. For molecules in the vicinity of metallic surfaces, nonadiabatic coupling is known to play a dominant role in the transfer of energy from the system to its surroundings, which leads, among other phenomena, to line broadening in spectroscopy and vibrational energy-loss in molecule-surface scattering.[6–11] The current explanation of these phenomena resides in the breakdown of the Born-Oppenheimer approximation, which poses that the electron react instantaneously to any nuclear motion. While the molecule is vibrating the electrons at the surface begin to adapt to the new local environment at finite speed and lag behind the molecular motion.[7] When the charge lags sufficiently behind the vibrating molecule, electron-hole pairs are created in the metal conduction band, a phenomenon sometimes called "electronic friction."

Several authors proposed perturbative expressions for treating the effect of electron-hole pair coupling.[11–20] In particular, Puska and Nieminen[13] introduced a model based on the dephasing of the electronic wave function at the Fermi level to estimate lifetimes. This model was also pushed forward more recently by Echenique and co-workers[20] and by Juaristi and co-workers,[11] among others. Another important approach, based on the dynamic self-energy for a vibrational mode of interest, was introduced and developed by Persson and co-workers.[12,14] A similar expression was obtained by Head-Gordon and Tully, who proposed a cluster-based single Hartree-Fock determinant procedure to evaluate the lifetimes,[16,17] which was further refined to better treat extended systems.[19] All these models define lifetimes in a site-local picture and focus on the first excited vibrational state, typically under the harmonic approximation. The lifetime is generally defined as

$$\tau_{vib} = (\Gamma_{1\to 0} - \Gamma_{0\to 1})^{-1}, \tag{1}$$

where $\Gamma_{1\to 0}$ is the transition rate from the first excited to the ground vibrational state and $\Gamma_{0\to 1}$ is an upward rate, related to the former by detailed balance (see below).

When performing dissipative vibrational dynamics, e.g., ladder climbing driven by tunneling electrons[21] or by infrared laser pulses,[22] however, lifetimes for and transition rates between all states need to be considered. The lifetime of higher excited states in the typically used single-mode, site-local harmonic approximation leads to one-phonon selection rules $\Delta n = -1$ for relaxation, and excited-state transition rates which scale linearly with the vibrational quantum number,[17,22] i.e.,

$$\Gamma_{n\to n-1} = n\Gamma_{1\to 0}. \tag{2}$$

For strongly coupled systems where the quantum numbers are not well defined, and for corrugated potential energy surfaces with multiple minima, this approximation fails.

We thus introduced recently[23] a position-dependent state-to-state transition rate model to circumvent these limitations, which relies on a certain number of simplifications. In particular, this rate model was based on embedding theory using a simple, jelliumlike embedding density. It has been argued that jellium-type (free electron gas) embedding models underestimate the amount of electronic damping when compared to self-energy calculations using first-principles, gradient-corrected density-functional theory.[24] In order to support or disprove the generality of this statement, it is a first objective of this paper to compare embedding/jellium-type models with first-principles methods for hydrogen on Pd(111). A second goal is to go beyond the jellium-type approaches but still adapt an embedding model, by using more realistic embedding densities which are derived from gradient-corrected density functional theory (DFT) calcula-

tions. Finally, first-principles calculations in the framework of dynamic self-energy theory will be used to calculate harmonic lifetimes for selected reference sites which are then used, in semiempirical fashion, to *calibrate* the embedding models. The goal is to obtain good representations of the global behavior of electronic friction, and to calculate anharmonic transition rates for H/Pd(111). Furthermore, the rates arising from different models will be used in dynamical calculations within open-system density matrix theory to enforce subsurface adsorption of H atoms, starting from an adsorbed state, by ladder-climbing induced by a sequence of infrared laser pulses.

The paper is organized as follows. In Sec. II we will describe the various methods to calculate the electronic damping rates, and the dynamical simulations using the open-system density matrix approach, respectively. In Sec. III B we present results for the transition rates in various models, and their performance in IR-driven vibrational dynamics in Sec. III C. Section IV concludes this work.

II. THEORY

A. Transition rate model

1. General expression

We study the case of an adsorbate, hereafter called the subsystem, located in the vicinity of a metallic surface. The subsystem vibrational dynamics is affected by energy dissipation due to electron-hole pair coupling. The state-to-state transition rates can be evaluated perturbatively using Fermi's Golden Rule for the nonadiabatic coupling elements.[12,14–19] At $T=0$, the transition rate is

$$\Gamma_{n'\to n} = \frac{2\pi}{\hbar}\sum_{i,f} |\langle n|\langle f|\hat{W}|i\rangle|n'\rangle|^2 \delta(E_i - E_f), \tag{3}$$

where $E_i(E_f)$ is the energy of the initial (final) vibronic state and $\delta(E_i - E_f)$ is the Dirac delta-function, ensuring energy conservation. The total wave function is represented as a product of vibrational and electronic states. States $|n\rangle$ and $|n'\rangle$ are associated with the vibrational degrees of freedom, while $|i\rangle$ and $|f\rangle$ are the electronic initial and final states. The operator $\hat{W}$ that represents the electron-hole pair coupling is the kinetic energy operator of the subsystem, which is, for a monoatomic adsorbate with coordinates $q(=x,y,z)$ and mass m given as

$$\hat{W} = -\frac{\hbar^2}{2m}\left(\frac{\partial^2}{\partial x^2} + \frac{\partial^2}{\partial y^2} + \frac{\partial^2}{\partial z^2}\right). \tag{4}$$

To simplify the derivation, we assume that the contributions of each coordinate q to the total downward transition rate from state n' to n are decoupled, that is

$$\Gamma_{n'\to n} = \sum_{q=1}^{3} \Gamma^{(q)}_{n'\to n}. \tag{5}$$

In case of a molecular adsorbate with N_A atoms, we treat every atom separately and the sum in Eq. (4) consists of $3N_A$ terms. Note that only downward transitions are possible at $T=0$ and that there are no upward rates. At finite temperature T, upward transitions which are related to the downward rates by detailed balance come into play

$$\Gamma^{(q)}_{n\to n'} = \Gamma^{(q)}_{n'\to n} e^{-(\epsilon_{n'}-\epsilon_n)/k_B T}, \tag{6}$$

where k_B is the Boltzmann constant and $\epsilon_{n,n'}$ are vibrational energies.

2. First-principles theory of harmonic, site-local transition rates

Various ways have been suggested of how to evaluate the rate expression (3), under additional approximations. In a first-principles approach, a rate expression can be used in which the dynamical self-energy is evaluated.[14,16] The two main lines of research to do so express the latter in a plane-wave basis in the framework of density functional theory, as proposed by Persson and Hellsing,[12,14] Persson and co-workers,[18] and Tully and co-workers,[19] or alternatively by Hartree-Fock wave functions for a small cluster, as advocated by Tully and co-workers.[16,17] In most actual investigations, (i) periodic DFT calculations using gradient-corrected exchange-correlation functionals are used, (ii) a harmonic approximation is made for the adsorbate vibrations, and (iii) the separability of nuclear and electronic degrees of freedom in the nonadiabatic coupling element $\langle n|\langle f|\hat{W}|i\rangle|n'\rangle$ is assumed. In practice, an adsorption site on the surface is determined by geometry optimization, followed by normal mode analysis to obtain the harmonic frequency ω_q of mode q and the corresponding normal mode eigenvector, $\mathbf{R}_q$. Considering periodically repeated cells, one can work in the basis of Bloch states and rewrite expression (3) for the rate of the first excited vibrational state decaying to the ground state ($T=0$ K), under the separability approximation as[18]

$$\Gamma^{(q)}_{1\to 0} = \frac{2\pi}{\hbar}\sum_{f,i,\mathbf{k}} \left|\langle i\mathbf{k}|\frac{\partial \hat{H}}{\partial \mathbf{R}_q}|_0|f\mathbf{k}\rangle\right|^2 \times |\langle 1|\delta\mathbf{R}_q|0\rangle|^2 \delta(\varepsilon_{f,\mathbf{k}} - \varepsilon_{i,\mathbf{k}} + \hbar\omega_q). \tag{7}$$

Here, i is an occupied and f an empty band index, $\mathbf{k}$ is a wave vector of the Brillouin zone, and $\varepsilon_{n,\mathbf{k}}$ are band energies at k-point $\mathbf{k}$. Further, $\frac{\partial \hat{H}}{\partial \mathbf{R}_q}|_0$ is the derivative of the electronic Hamiltonian with respect to the qth normal mode coordinate at the position of the equilibrium geometry, which can be evaluated by finite differences. (Note that second derivatives of the electronic wave function with respect to nuclear coordinates have been neglected.) The nuclear matrix element $\langle 1|\delta\mathbf{R}_q|0\rangle$ is given by $\sqrt{\frac{\hbar}{2m_q\omega_q}}$ in the harmonic oscillator approximation. Finally, the delta function can be approximated by a Gaussian of width σ, and the transition rate is then determined from the condition $d\Gamma^{(q)}_{1\to 0}/d\sigma = 0$. These procedures are detailed elsewhere[18] and have proven to give excellent results. Equation (7) will be referred to below as the "first-principles" method.

3. Rate expressions based on embedding theory

Puska and Nieminen[13] have proposed related expressions for electronic friction and relaxation rates, also advocated by

Hellsing and Persson[14] and more recently by Juaristi and co-workers,[11] based on scattering properties of the Kohn-Sham wave function of an atom embedded in a free electron gas. Accordingly, in the harmonic approximation,

$$\Gamma_{1\to 0}^{(q)} = \left\{ \left(\frac{3\hbar}{m}\right)\left(\frac{4}{9\pi}\right)^{1/3} \sum_{l=0}^{\infty} (l+1)\sin^2[\delta_{l+1}(\epsilon_F) - \delta_l(\epsilon_F)] \right\} r_s^{-2}. \tag{8}$$

The phase shifts at the Fermi level, $\delta_l(\epsilon_F)$, are tabulated elsewhere.[13] The electron gas parameter r_s is

$$r_s = \left(\frac{3}{4\pi\rho_{emb}}\right)^{1/3}, \tag{9}$$

where ρ_{emb} is the embedding density. For a homogeneous electron gas, ρ_{emb} and r_s are constants. In a real system, in particular at surfaces the embedding density ρ_{emb} is a function of coordinates (x,y,z) of the atom.

It has been suggested[23] to generalize Eq. (8) to

$$\Gamma_{n'\to n}^{(q)} = \gamma^{(q)} \left| \langle n' | \rho_{emb}^{1/3}(x,y,z) \frac{\partial}{\partial q} | n \rangle \right|^2. \tag{10}$$

The prefactor $\gamma^{(q)}$ in Eq. (10) can be interpreted as a scaling factor. For (i) the free-electron gas embedding model, (ii) specializing to the case $n'=1$ and $n=0$, and (iii) treating the vibrations as harmonic, we have

$$\left| \langle n' | \rho_{emb}^{1/3} \frac{\partial}{\partial q} | n \rangle \right|^2 = \frac{m\omega_q}{2\hbar} \left(\frac{3}{4\pi r_s^3}\right)^{2/3} \tag{11}$$

and therefore by comparing Eq. (10) with Eq. (8),

$$\gamma^{(q)} = \left(\frac{8\hbar^2}{m^2\omega_q}\right)\left(\frac{\pi}{3}\right)^{1/3} \sum_{l=0}^{\infty} (l+1)\sin^2[\delta_{l+1}(\epsilon_F) - \delta_l(\epsilon_F)]. \tag{12}$$

Therefore, by construction, in the harmonic approximation and the free-electron gas limit with the density defined by Eq. (9), Eq. (10) gives the result Eq. (8).

We can determine the scaling factor $\gamma^{(q)}$ alternatively by adjusting it to match the first-principles limit by construction. Let us suppose that we know, from the first-principles approach, for a particular mode and adsorption site a harmonic transition rate $\Gamma_{n'_{ref}\to n_{ref}}^{(q),ref}$ connecting two reference states n'_{ref} and n_{ref}. This can be, for example, the rate from the first excited state of H vibrating in the fcc surface site of Pd(111) in $q=z$ direction, to the ground vibrational state (see below). From Eq. (10), we then have

$$\gamma^{(q)} = \frac{\Gamma_{n'_{ref}\to n_{ref}}^{(q),ref}}{\left| \langle n'_{ref} | \rho_{emb}^{1/3}(x,y,z) \frac{\partial}{\partial q} | n_{ref} \rangle \right|^2}. \tag{13}$$

By construction, the scaling factor Eq. (13) reproduces the first-principles reference rate. Of course, any other reference might be used instead, e.g., experimental transition rates or lifetimes for the, say, perpendicular and parallel vibrations of H in a Pd(111) fcc site if available.

The derivation presented in our previous work relies on a certain number of simplifications, starting with the separation of the nuclear and electronic degrees of freedom. The "first-principles" expression is based on the free electron gas (FEG) model, as characterized by parameter r_s in Eq. (8). For an atom in the vicinity of a metallic surface, the FEG parameter depends of the position of the embedded atom at the surface. This idea was first introduced by Juaristi *et al.* for the purpose of calculating friction coefficient for classical dissipative dynamical simulations of atoms at metallic surfaces.[11] In this context, the function $\rho_{emb}^{1/3}(x,y,z)$ appears naturally in Eq. (8) to include the inhomogeneity of the electron density cloud at the surface. Specializing on the first excited state along a chosen harmonic mode, the "first-principles" model (8) and the perturbative approach [Eq. (10)] can be connected so that the latter reproduces the former in that particular limit. The numerical comparison with the model of Persson and co-workers[12–14,18] shows convincingly that the generalization of Eqs. (8)–(10) yields results of great accuracy, at least for the system studied here.

4. Three different embedding-based methods to calculate vibrational lifetimes

In the following, we will use, besides the "first-principles model" (7) within the harmonic approximation, three other methods which are based on the more approximate, but general embedding expression Eq. (10). These methods differ in their choice of the scaling factor $\gamma^{(q)}$ and the embedding density $\rho_{emb}(x,y,z)$.

The simplest approach is to use a jelliumlike, constant electron density inside the metal, while for atoms outside the jellium some z dependence can be introduced. The z dependence is introduced by noting that far from the surface, in the asymptotic limit for z, the electron density of a metal is equal to[23]

$$\rho_{emb}(x,y,z) = \rho_0 e^{-2\sqrt{2I}z}, \tag{14}$$

where I is the metal work function, and $\rho_0 = \frac{3}{4\pi r_s^3}$ is the associated free electron gas density for a given Wigner-Seitz radius r_s. This simple model, called "jellium" model in what follows, was used in our previous work[23] in conjunction with the (harmonic) scaling factor (12), to calculate *anharmonic* transition rates according to Eq. (10).

The jellium model neglects lateral variations of the embedding density. A more realistic model can be obtained using the electronic density of the metal $\rho(x,y,z)$,[11,20,25]

$$\rho_{emb}(x,y,z) = \rho(x,y,z). \tag{15}$$

The latter can be determined from a single periodic DFT calculation at all positions above and below the metal surface. This choice for ρ_{emb}, when still used in conjunction with the scaling factor (12), will be called the "metal" (density) model in the following.

The latter model relies on the assumption that the presence of the adsorbed species in the vicinity of the surface does not significantly modify the electronic density of the metal. To circumvent this limitation, we can define a more refined model for the embedding density. The idea is to place

an embedded atom at different positions above and below the metal surface, and to look at the density at the cusp defining the position of the nucleus, $\rho_{tot}(x,y,z)$. The relative value of the embedding density, $\rho_{emb}(x,y,z)$, is then obtained by removing the cusp density value of the free atom, ρ_{free}, i.e.,

$$\rho_{emb}(x,y,z) = \rho_{tot}(x,y,z) - \rho_{free}. \tag{16}$$

The absolute value of the embedding density is then obtained by normalizing the state-to-state transition rate of Eq. (10) to match the desired lifetime of a reference state, i.e., by using the scaling factor $\gamma^{(q)}$ as defined in Eq. (13). This procedure introduces some arbitrariness in the definition of the embedding density but includes the perturbation of the electronic density of the metal surface. This is the third method to be tested below, which will be referred to as the "perturbed" model.

B. Dynamical simulations

In the following, IR-laser driven vibrational dynamics in the presence of vibrational relaxation will be considered for H/Pd(111). To perform dynamical simulations, the subsystem dynamics will be treated using the reduced density matrix formalism, in which the effects of the surface are considered implicitly.[26] The reduced density matrix is obtained by tracing out the contributions of the environment from the total density matrix of the full system. Energy and phase relaxation due to the proximity to the metallic surface are included via the perturbative transition rate models described above. The subsystem dynamics will be steered in a desired direction by rationally designed short, intense laser pulses. The time evolution of the reduced density operator, $\hat{\rho}(t)$, obeys the Liouville–von Neumann equation.[26] By (i) expressing the density operator in the basis of the vibrational eigenstates $\psi_n = |n\rangle$ of the vibrating H atom, (ii) using the semiclassical dipole approximation to treat the coupling of these vibrations to an external field, and (iii) employing so-called Lindblad operators[27] to enforce environment-induced, dissipative transitions between the vibrational levels with rates $\Gamma_{n\to n'}$, the time evolution of the reduced density matrix elements becomes[22,28,29]

$$\frac{d\rho_{nn}}{dt} = -\frac{i}{\hbar}\sum_{p=x,y,z} E_p(t)\sum_i (\mu_{ni}^{(p)}\rho_{in} - \rho_{ni}\mu_{in}^{(p)}) + \sum_i (\Gamma_{i\to n}\rho_{ii} - \Gamma_{n\to i}\rho_{nn}), \tag{17}$$

$$\frac{d\rho_{n'n}}{dt} = -i\omega_{n'n}\rho_{n'n} - \frac{i}{\hbar}\sum_{p=x,y,z} E_p(t)\sum_i (\mu_{n'i}^{(p)}\rho_{in} - \rho_{n'i}\mu_{in}^{(p)}) - \gamma_{n'n}\rho_{n'n}. \tag{18}$$

Here, $\omega_{n'n} = (\epsilon_{n'} - \epsilon_n)/\hbar$ is the energy difference between states n' and n, E_p is the p^{th} component of the laser field, and $\gamma_{n'n} = 1/2\Sigma_l(\Gamma_{n'\to l} + \Gamma_{n\to l})$ is a dephasing rate, arising from the energy relaxation processes. Further, $\mu_{ni}^{(p)} = \langle n|\mu^{(p)}|i\rangle$ is the transition dipole moment associated with the p^{th} component of the dipole function $\mu^{(p)}$. The dipole moment function was obtained from cluster model calculations using density functional theory.[23] In the case studied here, the dynamics follows the direction perpendicular to the surface. Furthermore, the component of $\mu^{(p)}$ parallel to the surface is small in comparison to the perpendicular one. Thus, only the z component of the dipole moment was computed. The diagonal elements of the density matrix, ρ_{nn} in Eq. (17), represent the subsystem state populations, and the off-diagonal elements, $\rho_{n'n}$ in Eq. (18), represent coherences.

It must be mentioned that the spectral lines associated with the adsorbate vibrational transitions will appear as small features on the top of a much broader spectrum, which has its origin in the excitation of the continuum of electronic states. In theoretical simulations, it is extremely difficult to take into account the perturbation of the electronic density at the surface by the external electric field. Thus, this contribution is left aside in most theoretical treatments, as is the case here. It is postulated that the continuum absorption should not affect the control mechanism. On the other hand, the adsorbate vibrations and the surface electronic states are known to be strongly coupled. Inclusion of the perturbation to the electronic density in our model might change the dynamical behavior of the system. This said, the Lindblad dynamical semigroup approach and the perturbative treatment of the nonadiabatic coupling should account for most of the homogeneous line broadening of the resonant transitions. Thus, a significant part of the effect of the non-Born-Oppenheimer coupling on the adsorbate dynamics is already taken into account by our dissipation model.

III. RESULTS

A. Computational realization

1. Anharmonic subsystem eigenstates

We apply our transition rate models to study the dissipative dynamics of a single hydrogen atom adsorbed on a palladium (111) surface. The full-dimensional Hamiltonian of the subsystem is given by

$$\hat{H} = -\frac{\hbar^2}{2m}\left(\frac{1}{\sin^2(\alpha)}\frac{\partial^2}{\partial s_1^2} - \frac{2\cos(\alpha)}{\sin^2(\alpha)}\frac{\partial^2}{\partial s_1 \partial s_2} + \frac{1}{\sin^2(\alpha)}\frac{\partial^2}{\partial s_2^2} + \frac{\partial^2}{\partial z^2}\right) + V(s_1,s_2,z). \tag{19}$$

Here, s_1 and s_2 are skewed coordinates parallel to the surface chosen to follow the 1×1 unit-cell borders, at an angle $\alpha = 60°$ and coordinate z defines the distance from the surface. Figure 1(a) shows a cartoon of the hydrogen-palladium system. The cartesian and skewed in-plane coordinates, as well as the angle α are defined in Fig. 1(b). The transition rates were computed along the rotated cartesian coordinates q_d and q_p, which better follow the nodal structure in the 1×1 unit cell. For more details, the reader is referred to our previous work.[23] We use the potential energy surface of Osawa *et al.*[30] to describe the interaction of the hydrogen atom with the surface. The Osawa surface was obtained from periodic DFT calculations, similar to ours as reported below.

The time-independent Schrödinger equation was solved using the variational method. A linear combination of tensor-

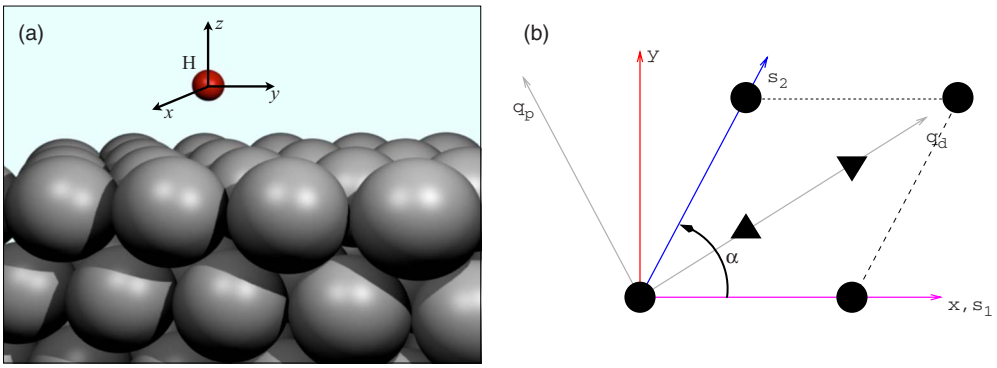

FIG. 1. (Color online) Schematic representation of the dynamical system. Panel (a): Cartoon of the H/Pd(111) system showing the three cartesian axes. Panel (b): Coordinates describing the hydrogen atom position on the surface. The 1×1 unit cell is represented by balls, triangles, and inverted triangles for the first, second and third palladium atom layer, respectively. See text for more details.

products of one-dimensional basis functions was used as a trial function. Coordinate $s_1(s_2)$ was represented in a basis of 25 plane-wave discrete variable representation (exp-DVR) functions[31] on the interval spanned by the 1×1 unit-cell. A basis of 100 sinc-DVR functions[32] on the range $[-4.5,2.0]$ Å was used for the z coordinate [Fig. 1(a)]. The 392 lowest eigenstates up to 7600 cm^{-1} above the potential energy minimum were extracted using an implementation of the coupled two-term Lanczos algorithm with full reorthogonalization.[33,34] All states were used in the dynamics calculations in Sec. III C.

The potential energy minimum corresponds to the fcc adsorption site ("fcc site"). Besides that, other important minima to be considered below are the hcp adsorption site which is only about 300 cm^{-1} higher in energy ("hcp site"), the octahedral subsurface adsorption site about 2500 cm^{-1} above the global minimum ["O_h (sub) site"], and, finally, the octahedral bulk absorption site ["O_h (blk) site"], about 3200 cm^{-1} above the minimum (see Fig. 1 in our previous paper[23] and also Fig. 2 below). All of these minima support perpendicular ("z") and parallel modes ("p"), the latter being doubly degenerate. The fundamental frequencies at the fcc center are 922 cm^{-1} for the perpendicular mode and 717 cm^{-1} for the parallel mode. In the subsurface octahedral

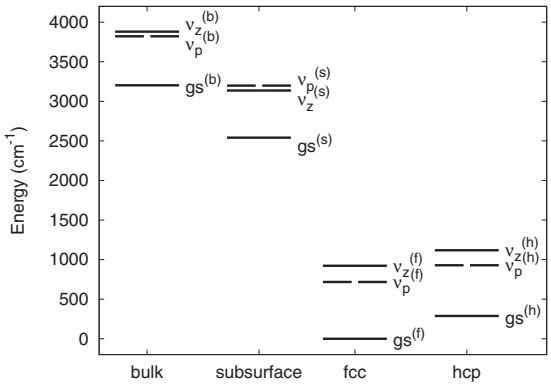

FIG. 2. Ground and first excited vibrational states of the full-dimensional Hamiltonian sorted according to the site where they are localized. The labels $^{(b)}$ and $^{(s)}$, refer to the bulk and subsurface octahedral site, and the labels $^{(h)}$ and $^{(f)}$ to the hcp and fcc adsorption sites, respectively.

cavity, the energy ordering is reversed, with 606 and 638 cm^{-1} for the parallel and perpendicular mode frequencies, respectively. In the bulk site, we find a very similar transition frequency for the perpendicular mode (640 cm^{-1}), but the parallel mode remains slightly higher in energy (648 cm^{-1}). For a deeper analysis of the vibrational states of hydrogen on palladium, the reader is referred to our previous work.[23] There it is also shown how the derivatives of the vibrational wave functions with respect to coordinate q as required in (10) were done.

2. Electronic structure calculations

To calculate embedding densities, density functional calculations were performed with the plane-wave based VASP code,[35,36] using the PW91 exchange-correlation functional.[37] The substrate was represented by a six-layer slab containing only one atom each (1×1 supercell). The reciprocal space was sampled with an automatically generated $15\times15\times1$ Monkhorst-Pack grid.[38] In the relaxation process, the atoms of the three top layers of the slab were free to move, their coordinates changed until a force of 0.01 eV/Å or less was reached. We then extracted the self-consistent electronic density $\rho(x,y,z)$ of the system, which was used as the embedding density in the "metal" model [see Eq. (15)]. The calculation of the "perturbed" density [Eq. (16)] was performed exactly at the same level of accuracy by including a hydrogen atom and varying its position along the z-coordinate, while maintaining the palladium atoms fixed. This was done for four positions of the hydrogen atom in the (x,y) plane: the fcc, hcp, top and bridge sites. For each site, ten points in the range $[-4.5,2.0]$ Å were used to calculate the perturbed density. Exploiting the C_{3v} symmetry of the system to generate a denser set of points, the perturbed metal density was interpolated on the resulting grid using three-dimensional (3D) natural splines.

To compute first-principles harmonic lifetimes according to Eq. (7), we preferred to use a bigger supercell ($2\times2\times6$) in order to avoid effects arising from the periodically repeated cells. These include attraction or repulsion of the adsorbate in adjacent cells, as well as possible constraints in the lateral motion, along the diffusion coordinate. An ionic relaxation was first performed to obtain the equilibrium geometry of the system and in particular to get a realistic ad-

sorption distance. A normal mode analysis was then performed as outlined earlier. Two modes of special interest are the perpendicular mode of H, adsorbed in the fcc site, and the perpendicular mode of H in the octahedral subsurface site. Both correspond to normal modes with coordinates $\mathbf{R}_q$ which show an almost pure H motion along z, with only minor contributions from the surrounding Pd atoms. The corresponding harmonic vibrational frequencies are $\omega_z^{(f)}=976\ \mathrm{cm}^{-1}$ for the fcc adsorption site, and $\omega_z^{(s)}=565\ \mathrm{cm}^{-1}$ for the octahedral subsurface site—the anharmonic values of the previous section, obtained from the full potential surface, were 922 cm^{-1} and 606 cm^{-1}, respectively.

The matrix elements $\langle i\mathbf{k}|\frac{\partial\hat{H}}{\partial\mathbf{R}_q}|f\mathbf{k}\rangle$ in Eq. (7) were evaluated by finite differences and the delta function was approximated by a Gaussian of width $\sigma=0.2$ eV, chosen according to the criteria given in Sec. II A 2. As discussed in the work of Lorente and Ueba,[21] the k-point sampling is critical in order to obtain reliable results. We used a $7\times7\times1$ grid, which gives a good sampling according to references 19 and 21.

Two vibrational lifetimes have been calculated by the first-principles method: For the perpendicular mode in the fcc site, we obtain a lifetime $\tau=1/\Gamma_{\nu_z^{(f)}\to gs^{(f)}}$ of 393 fs. For the octahedral subsurface site, we get $\tau=1/\Gamma_{\nu_z^{(s)}\to gs^{(s)}}=416$ fs. The first of these transition rates, $\Gamma_{\nu_z^{(f)}\to gs^{(f)}}$, has been used as the reference rate to calibrate the "perturbed" embedding-density model according to Eq. (13). The lifetimes will be discussed in more detail in Sec. III B 2.

B. Vibrational lifetimes from embedding-based methods

1. Embedding density

Before doing so, it is necessary to compare the different models introduced in Sec. II A 4 to calculate embedding densities. The "jellium" model is defined using constants $I=0.1881$ for the work function of Pd(111) and $\rho_0=\frac{3}{4\pi r_s^3}$ with $r_s=2.9$ (all in atomic units) for the density inside the metal. The jellium model is to some extent trivial (it is flat inside the surface and decays exponentially outside) and not shown here.

Figure 3 shows a two-dimensional cut of the embedding densities of the "metal" [Eq. (14)] and "perturbed" models [Eq. (15)]. The coordinate z has its zero defined as the first layer of palladium atoms (the black dots). The other coordinate is a linear combination of the two skewed coordinates that bisects the 1×1 unit cell through all the highly symmetric points above and below the surface (fcc, hcp, bridge, and O_h). For clarity, fcc (f) and hcp (h) adsorption sites, as well as subsurface (s) and bulk (b) absorption sites are indicated in the left panel of Fig. 3.

The electronic density of the free metal shown on the left rises slowly when coming down the z direction along the hydrogen absorption path at the fcc center (at about $\frac{s_1+s_2}{2}=3.29$ Å). After reaching a saddle point at the surface the embedding density goes down slowly to reach a local minimum a little below the subsurface octahedral site, at about $z=-1.2$ Å. Another local minimum can be seen at the end of the unit-cell and a depth of $z=-3.5$ Å, which is a bit lower than the bulk octahedral site. The electronic density also increases steeply when approaching the palladium atoms.

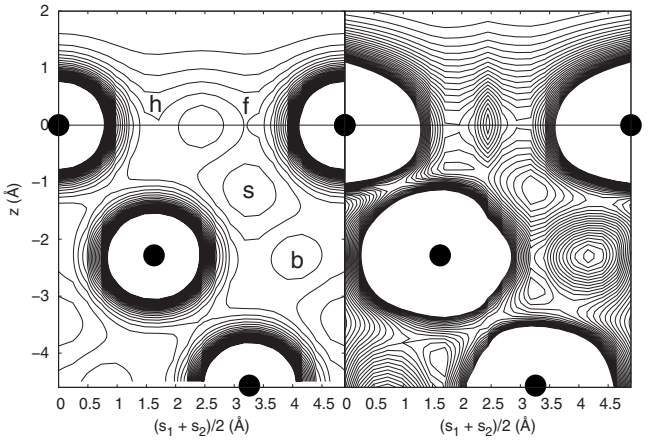

FIG. 3. Comparison of the embedding density for a hydrogen atom on a palladium (111) surface. The dots represent the palladium atoms and the first metal layer defines the zero of the surface. In the left panel, fcc (f) and hcp (h) adsorption sites, as well as subsurface (s) and bulk (b) absorption sites are indicated. The contours range from 0 to 0.2 a_0^{-3} and are separated by 0.006 666a_0^{-3} increments. Left panel: Free metal density. Right panel: Perturbed metal density.

The comparison to the perturbed density model (right panel) is striking. First, the embedding density rises much more quickly when the hydrogen atom approaches the surface. The local minima and maxima, as well as the saddle points, are indeed located at about the same position as for the free metal density case, but perturbed density gradients are much larger at all other positions. The steeper fluctuations of the perturbed density can be explained by: (1) the increase in the number of electrons by volume due to the addition of the hydrogen atom in the system, (2) the increase of the electron density in the vicinity of the hydrogen atom to stabilize the positive charge as it approaches the palladium atoms. The first point does not cause any problem since the embedding density is scaled to a desired value using Eq. (13). Furthermore, the high values of the embedding density correspond to geometries that are not energetically accessible, and that will consequently not affect the transition rates. Also, the perturbed density does not appear to be isotropic at the vicinity of the palladium atoms. This can be rationalized by the fact that the environment is not of spherical symmetry around the atoms. This could also be an artifact of to the relatively small number of sampling points used for generating the perturbed metal density.

2. Lifetimes

First excited states. In Table I we give the lifetimes associated with the different embedding-density models for the first excited state of the perpendicular mode of the hydrogen atom, obtained by integrating Eq. (10). The lifetimes are sorted according to the ad-or absorption site in which their maximum amplitude is located, which was determined by direct inspection of the wave functions. It is important to keep in mind that these assignments are approximate, as all degrees of freedom of the system are strongly coupled and the wave functions are only partially localized in the local

TABLE I. Perpendicular mode lifetime of a hydrogen atom in the stable ad- and absorption sites of a palladium (111) surface for three different embedding-density models, and, for selected cases, for the first-principles approach (see text for details). All lifetimes are given in femtoseconds. The label "mode" refers to the state-to-state lifetime in the decoupled mode picture. The label "sum" refers to the state lifetime including all dissipation channels. In the lowest row, the vibrational energies (in cm^{-1}) relative to the ground state of the local center are given.

	fcc site		hcp site		O_h (sub) site		O_h (blk) site	
Model	Mode	Sum	Mode	Sum	Mode	Sum	Mode	Sum
Jellium	1349	1057	2513	1004	389	389	367	367
Metal	370	302	1191	323	373	373	350	350
Perturbed	392	324	1270	341	526	526	451	451
First principles	393				416			
Frequency	922		829		606		648	

potential wells. The label "mode" refers to the state-to-state lifetime, obtained by inverting the state-resolved transition rate from the first excited state to its associated local minimum. The label "sum" refers to the lifetime including the contribution of all decaying channels. That is, we sum the transition rates of all lower-lying states, $\Gamma_k^{(sum)}=\Sigma_{n=1}^{k-1}\Gamma_{k\to n}$. For example, the first perpendicular mode excited state centered at the fcc site lies fifth in the energy spectrum. Thus, the "sum" lifetime is given by $\tau_4=\frac{1}{\Gamma_4^{(sum)}}=(\Gamma_{4\to 3}+\Gamma_{4\to 2}+\Gamma_{4\to 1}+\Gamma_{4\to 0})^{-1}$. States {2, 3} correspond to the degenerate parallel mode and the state-to-state lifetime from the first perpendicular mode to the parallel mode is about 3.3 ps. The transition to the hcp site (state 1) is much longer, at about 400 ps. The sum lifetime is dominated by the contribution of the $4\to 0$ transition, but coupling to the parallel mode reduces it to about 302 fs. The discrepancy between the two lifetime values is a good indication of the anharmonicity of the wave functions and the degree of coupling between the different modes. For comparison, we give in Table I also the two first-principles rates obtained in Sec. III A 2

From the Table, the following conclusions can be drawn:

(i) When comparing the "first principles" to the "perturbed" model lifetimes for the fcc adsorption and subsurface O_h sites, we note first of all that they are, by construction, (almost) identical for the former, but deviations in the order of 20% occur for the latter. Since the first-principles subsurface lifetime has not been used for calibration, this is the order of magnitude which we expect for the accuracy of the (nonjellium) embedding schemes, relative to the first-principles approach. Of course, the harmonic first-principles approach has also limitations.

(ii) Most of the computed lifetimes are in the range of a few hundred fs, some extending into the ps regime. This is quite typical for adsorbate vibrations at transition metal surfaces.[11–20]

(iii) One can see that, for all three embedding-density models, the lifetimes in both the subsurface and the bulk octahedral sites are very similar. Only the perturbed density model yields slightly longer lifetimes. Further, the difference between the two octahedral absorption sites is a bit larger than for the two other models. This is possibly due to the larger gradient of the embedding density inside the surface in the perturbed metal model than in the other two. In all cases, though, one can see that the "sum" and "mode" lifetimes are almost equal. This indicates that, inside the surface, the first excited state of the perpendicular mode is almost harmonic and does not couple to the lateral mode.

(iv) This is not the case for the vibrational states of the hydrogen atom above the surface, in fcc and hcp adsorption sites. First, the lifetimes are significantly longer for the jellium model than for the free metal model for both the fcc (1.35 ps vs 370 fs) and hcp sites (2.51 ps vs 1.19 ps). This is an indication that the embedding density is much too thin outside the surface in that crude model. Also, the lifetime appears to be much longer in the hcp site than in the fcc site for both models, when looking only at the "mode" lifetime. This effect is more pronounced when using the free metal density in Eq. (10). When including all dissipative channels, though, the lifetimes in the fcc and hcp centers become much more similar (302 and 323 fs, respectively, for the free metal model). The trend for the lifetimes is even slightly reversed for the jellium model (1.06 and 1.00 ps for the fcc and hcp centers, respectively). This is indeed an indication of strong intermode coupling and large anharmonicity, even for the first excited state. This effect is strongest for the hcp site, because the wave function is more diffuse inside this well. This is due to the very low diffusion barrier between the two adsorption sites, with a classical value on the same order of magnitude as the energy level.[23]

(v) While the difference between the simple "jellium," and the more sophisticated "metal" and "perturbed" embedding models can be very substantial, the difference between these latter two are generally not huge, in particular for the adsorption (rather than absorption) sites: The "perturbed" model gives typically slightly higher lifetimes than the "metal" model. As an example, the perpendicular mode in the fcc adsorption site has a lifetime of 392 fs in the "perturbed" model case, compared to 370 fs for the "metal" case. The latter is in some sense more "*ab initio*" since no semiempirical scaling is involved. For the perpendicular subsurface O_h vibration, the "metal" density model predicts a lifetime of 373 fs which agrees even better with the first-principles value of 416 fs, than the "perturbed" model (526 fs). This is encouraging, since the "metal" model requires only the density of the naked Pd surface which can be ob-

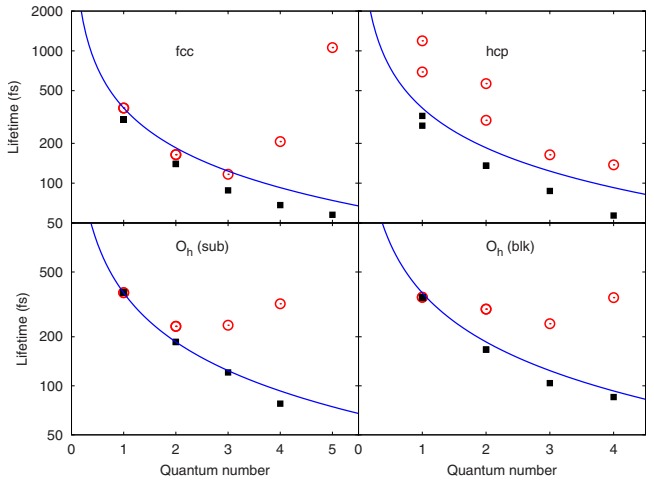

FIG. 4. (Color online) Rate of the perpendicular mode overtones for H on Pd(111) in different sites obtained using the pure metal density for the embedding density. The red circles are the state-to-state lifetimes and the total lifetimes are represented by black squares. The quantum numbers were obtained by visual inspection of one-dimensional cuts of the wave functions integrated on the parallel mode coordinates.

tained from a single periodic DFT calculation, in contrast to the "perturbed" model which requires many DFT calculations on a 3D grid.

We finally note that according to Table I, the first-principles lifetime can be longer or shorter than the lifetimes obtained with embedding schemes. This depends on which model was used for the embedding density, and also if the atom is adsorbed or absorbed. Hence, the statement made by Luntz *et al.*,[24] according to which models based on atoms embedded in a homogeneous electron gas generally underestimate the amount of electronic friction, is not supported by our calculations.

Higher excited states. Concerning now higher-excited state lifetimes, according to Eq. (2) the transition rates increase linearly with initial quantum number, n in the harmonic approximation, or, equivalently, the lifetime $\tau_{n'\to n}$ scales as $\tau_{n'\to n}=\frac{1}{n'}\tau_{1\to 0}$. Figure 4 shows the lifetimes for vibrational progressions of the perpendicular mode centered at different sites, in our anharmonic, coupled approach. The red circles and black squares represent the "mode" and "sum" lifetimes, respectively, and the solid line is the ideal harmonic scaling. The lifetimes were obtained using the free metal density, but similar trends are observed for the other embedding-density models. [Selected "mode" lifetimes for higher excited states for all three models (jellium, metal, and perturbed), are also shown in Fig. 5.]

From Fig. 4 we see that at the fcc center, the state-to-state lifetimes follow approximatively the harmonic scaling up to the third excited state. The fourth and fifth quanta appear strongly off the ideal scaling, the latter even having a longer lifetime than the $1\to 0$ transition. This is in stark contrast with the "sum" lifetime, which keeps going down regularly as the vibrational quantum number increases. Strong coupling between the modes and large anharmonicity are again the main responsible for the discrepancies between the life-

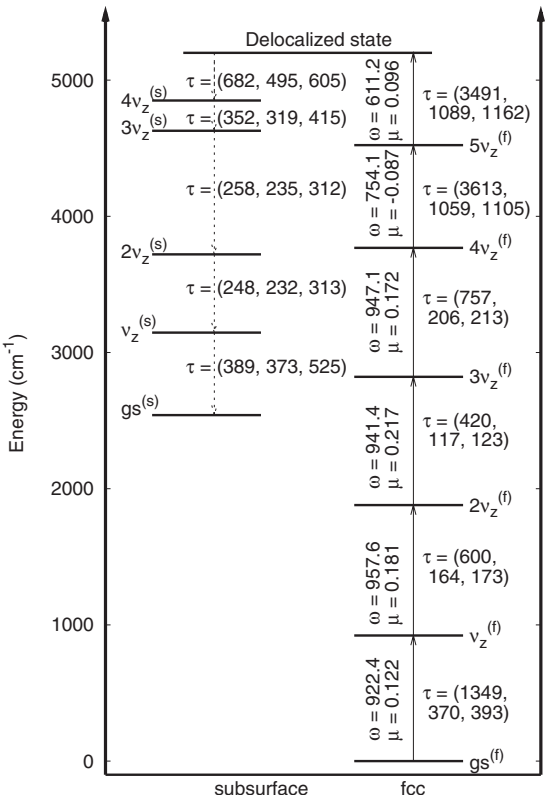

FIG. 5. Selected states involved in the enforced reaction path for the full-dimensional Hamiltonian. The transition dipole moments μ (in ea_0), the state-to-state lifetimes τ (in fs) and the transition energies ω (in cm^{-1}) as well as the state assignments are noted beside the transitions. The labels $^{(s)}$ and $^{(f)}$ refer to the subsurface and fcc adsorption sites, respectively. The state-to-state lifetime is given in parenthesis for the jellium model, the free metal model and the perturbed metal model, respectively.

times. For the octahedral cavities in the bulk and in the subsurface, the progression breaks even earlier for the "mode" lifetime, whereas the "sum" lifetimes behaves again more regularly.

A peculiarity arises at the hcp center, where the assignment of the first excited state is not unambiguous. The two states which can pretend to the label have some nodal structure in both the fcc and hcp wells, and have about the same energy. The full-dimensional vibrational eigenstates extracted here are linear combinations of motions parallel and perpendicular to the surface. This renders their assignments dubious and thus both lifetimes are reported in Fig. 4 for the two first vibrational quanta. As was the case for the other sites, the scaling is not respected by the state-resolved lifetimes, but the transition rates have a more regular behavior when all dissipation channels are included.

Parallel modes. The lifetimes for the mode parallel to the surface are reported in Table II for different sites. The lifetime in the fcc adsorption site is similar but slightly smaller than the perpendicular mode for all three embedding-density models. The lifetimes in the hcp site are also slightly longer than those in the fcc site in all three cases. Interestingly, the lateral motion in both the subsurface and bulk octahedral sites are very similar in magnitude for the jellium model

TABLE II. Parallel mode lifetime of a hydrogen atom in the stable ad- and absorption sites of a palladium (111) surface for different embedding-density models. In the lowest row, the vibrational energies (in cm^{-1}) relative to the ground state of the local center are given. See Fig. 1 and text for more details.

	fcc site		hcp site		O_h (sub) site		O_h (blk) site	
Model	Mode	Sum	Mode	Sum	Mode	Sum	Mode	Sum
Jellium	1130	1130	1366	1304	289	289	291	291
Metal	327	326	395	376	279	279	277	277
Perturbed	350	349	428	406	391	391	362	362
Frequency	717		640		638		640	

(289 and 291 fs, respectively), and for the free metal model (279 and 277 fs, respectively).

Again, it appears that the simple jellium model captures the main features of the embedding density inside the metal. The perturbed metal density shows a small difference between the two octahedral cavities (391 fs vs 362 fs). Further, these lifetimes are much longer than in the other two models. This is probably an artifact of the method we proposed for calculating the perturbed metal density. It must also be emphasized that in the "perturbed" model the perpendicular fcc mode has been used for the first-principles calibration, and none of the parallel modes. Note that, in contrast with the perpendicular mode, the "sum" and "mode" lifetimes are very similar for all three embedding-density models and all four metastable sites. This seems to indicate that the first excited state along this mode is not significantly affected by anharmonicity nor delocalization of the wave function.

C. Infared-laser driven subsurface absorption

We will now test the effect of the different state-resolved lifetime models on the laser-driven dynamics of a single hydrogen atom on a palladium (111) surface. It is believed that subsurface hydrogens are involved in heterogeneous catalysis at metal surfaces and that they are more reactive than the bulk hydrogens.[39–47] In a recent paper,[23] we proposed a strategy for controlling the selective population of the subsurface octahedral site. Since the subsurface states are not directly accessible from the vibrational ground state, we showed that an indirect path can prove the most efficient solution. The main idea is to excite the perpendicular mode at the fcc center up to a high-lying target state by vibrational ladder climbing. This intermediate, or target state is chosen because it decays with some probability toward the subsurface site.

Figure 5 shows schematically the desired reaction path. For better illustration, we show only selected "perpendicular" states, namely the fcc levels (labeled $k\nu_z^{(f)}$ or $\mathrm{gs}^{(f)}$) and the O_h subsurface states (labeled $k\nu_z^{(s)}$ or $\mathrm{gs}^{(s)}$). Here, "gs" denotes the vibrational ground state in a given site, and $k\nu_z$ the kth excited state, for vibration along coordinate z. The labels given here are by no means unique, since the different "modes" and the different sites are all strongly coupled. They merely serve as a tool to guide the intuition in understanding the intricate dynamics. Thus, although the parallel modes and levels localized in other minima are not shown in the figure, they were included in the dynamics. The same is true for all "delocalized states," the one used to connect subsurface and fcc adsorption wells being indicated in Fig. 5. The transition frequencies and the transition dipole moments are given for the states forming the vibrational ladder, outside the surface at the fcc center. The transition dipole moments are for the z components only, i.e., we assume laser pulses polarized perpendicular to the surface (see below). The transition dipole moments have been obtained from a dipole function which has been calculated using a cluster model and density functional theory.[23] As stated, we also show in the figure the state-to-state lifetimes in parenthesis for the jellium, the free metal, and the perturbed metal model, respectively. Note that the state-to-state lifetimes are shorter in the subsurface than at the surface for all three embedding-density models, however, the integral lifetimes can be substantially different because of the strong anharmonicity and the coupling between the states located at different ad- and absorption sites (see above). In all cases but the perturbed metal density, the "sum" lifetime is nonetheless smaller for the decay from the intermediate state to the subsurface site than to the surface. Further, the lifetimes of both the perturbed metal and the free metal models are significantly shorter than for the jellium model, for which the approach was originally developed. This should adversely affect the dynamics.

Figure 6 shows the short time evolution of the state population when the subsystem is forced along the reaction path described above by a z-polarized electromagnetic field E_z. A single pulse of the form,

$$E_z(t) = E_0 \sin^2\left(\frac{\pi(t-t_i)}{t_f - t_i}\right)\cos(\omega t), \tag{20}$$

starting at time $t_i=0$ and ending at time $t_f=500$ fs, was tailored to pump the population up the vibrational ladder. Here, E_0 is the field amplitude, chosen so that the field's average intensity is $I=10^{13}$ W/cm^2, i.e., $E_0=100$ MV/cm. The frequency ω was tuned at the average of the z-mode vibrational ladder frequencies, at 940 cm^{-1}.

From top to bottom, we see that there is very little difference in the intricate short-term population dynamics for the different embedding-density models. Energy is indeed very quickly pumped in the z-mode up to the fifth excited state, with a maximal yield ($\sim$7.5%) for the subsurface ground state $\mathrm{gs}^{(s)}$ at 100 fs for the jellium model. This yield is better than for the other two models, which can be easily rationalized by the fact that the lifetimes are much longer in that case

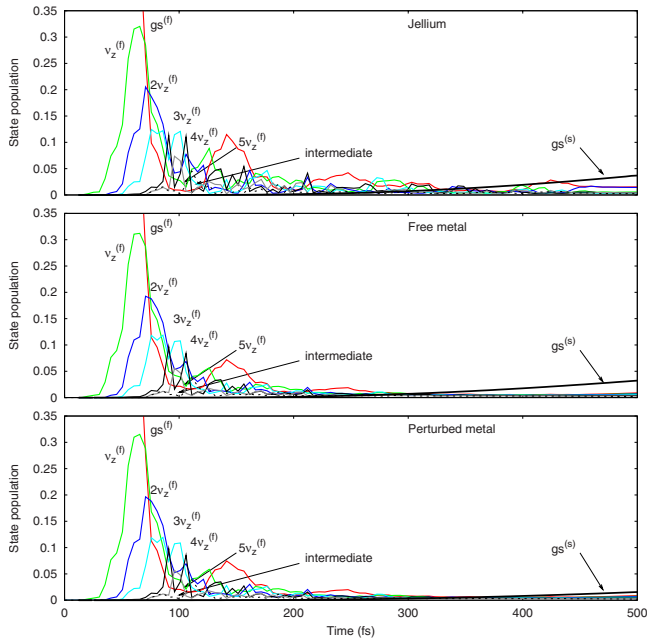

FIG. 6. (Color online) Comparison of the short-term dynamics for the selective subsurface absorption of hydrogen in the palladium (111) octahedral subsurface site. The average laser intensity is $I=10^{13}$ W/cm^2 for a single pulse of 500 fs duration tuned at a transition frequency of $\omega=940$ cm^{-1}.

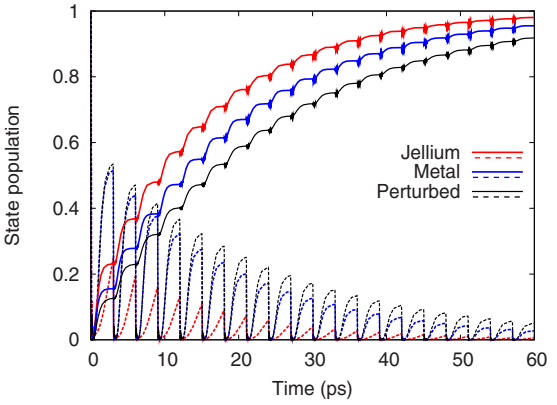

FIG. 7. (Color online) Selective subsurface absorption of hydrogen in the palladium octahedral subsurface site using laser distillation affected by our different dissipation models. The solid curves represent the subsurface ground state population and the dotted curves the fcc ground state population. The red, blue, and black curves are obtained with the jellium model, the free metal model and the perturbed metal model, respectively.

than for both the free and perturbed metal models. The large intensity of the pulse allows nevertheless to transfer significant population to the fourth z-overtone in both other simulations (about 5% in both cases). The fraction of population reaching the intermediate state (dashed line) is found similar to that of state $5\nu_z^{(f)}$ in all three models, only at a later time. The subsurface population at the end of the pulse is relatively modest for the jellium (4%) and the free metal models (3.5%), and is lower for the perturbed metal model (1.5%). This is due to the larger transition rate to the adsorbed sites than to subsurface for the latter embedding density. Thus, although it is possible to reach the intermediate target state with a comparable yield as in the other two models, the vibrationally excited atom preferably returns where it comes from, outside the surface.

The main strategy to bring the population in the subsurface does not rely on the transfer yield after a single pulse, however. Instead we exploit the fact that the subsurface ground state is quasistable to accumulate the population in the subsurface. The idea is to perturb the system using the pulse in Eq. (20), let the system relax for a short period, and collect the population that accumulates in the subsurface site. This idea is known as laser distillation.[48–50] We have thus performed series of the 500 fs pulses described above, followed by 2.5 ps periods. In Fig. 7 we show the population dynamics for the first 20 pump-dump sequences using the three different embedding-density models. Only the fcc ground state (dashed lines) and the subsurface ground state (solid lines) populations are shown. We can see that about 23.1% of the population is found in the subsurface after the relaxation period in the jellium model, which is significantly more than for both other embedding-density models.

This is simply due to the fact that the lifetimes are much longer in the former case, thus allowing to pump more energy in the perpendicular mode at the surface. The preferred decay channels lead to the subsurface site, and thus a significant transfer yield is obtained. In comparison, dynamics in the free metal model yields marginally above 15.5% population in the desired octahedral cavity. This is comparatively better than the dynamics in the perturbed metal embedding density, where only about 12.6% population transfer is obtained after the first pump-dump sequence although the lifetimes are slightly longer in the latter model. As already pointed out, the subsurface transition rates are smaller than the relaxation to the subsurface in this case, which justifies this behavior.

To characterize the convergence of the laser distillation mechanism, we fit the subsurface population at the end of each pulse-relaxation sequence, $P(t)$, to a simple exponential function of the form $P(t)=P_{\max}(1-e^{-Rt})$. Here, $P_{\max}$ is the maximal population attainable and R is the convergence rate. Interestingly, all three models yield a projected 99.6% subsurface population in the limit of an infinite number of pulses. The convergence rate, on the other hand, follows more tightly the ratio of the subsurface population after a single pulse. We find that the laser distillation converges at a rate of $R_J=0.0705/\text{ps}$ for the jellium model, and of $R_M=0.0533/\text{ps}$ for the metal density. The convergence ratio of $\frac{R_J}{R_M}=1.32$ compares fairly well with that of the single pulse yield of 1.49, but the correlation is not direct. The correspondence is much better between the two metal embedding-density models, with a ratio of $\frac{R_P}{R_M}=0.81$ for the laser distillation yield ($R_P=0.0428/\text{ps}$) and a ratio of 0.80 for the corresponding single pulse excitations.

The main conclusions are thus that dissipation can indeed be used to selectively populate the subsurface octahedral absorption sites of palladium with hydrogen atoms using simple infrared laser pulses, and that laser distillation should transfer quantitatively the population to the subsurface pro-

vided at least some atoms are dumped in the surface after a single excitation-relaxation cycle. Although the convergence rate toward the final target depends on the embedding-density models, the general dissipative dynamics and the final yield of the laser-driven subsurface absorption of hydrogen by laser distillation appears robust with respect to the definition of the embedding density.

IV. SUMMARY AND CONCLUSION

In conclusion, we have presented a state-resolved perturbative transition rate model for describing the nonadiabatic coupling of an adsorbate to a metal surface based on Fermi's Golden rule. The treatment relies on the embedding of the adsorbate in an effective ambient electron density due to the surface. Anharmonicity is included by evaluation of the gradient of the full-dimensional vibrational wave function with respect to each nuclear coordinate. The single-mode contributions to the lifetime are coupled through the embedding-density scheme.

We proposed three different embedding-density models: (i) the simple jellium model, neglecting electron density variations inside and parallel to the surface, (ii) the free metal electron density, which neglects the effect of the impurity on the electronic wave function of the metal, and (iii) the perturbed metal density, using a simple pointwise definition for the density. By comparison with the single-point *ab initio* model of Persson *et al.* it was found that the jellium model gives unphysically long lifetimes for an hydrogen atom adsorbed on a Pd(111) surface, but realistic estimates when the atom is found inside the metal. The state-resolved lifetimes obtained using the two other embedding-density models are on the other hand realistic and comparable in both case to the first-principles estimates. In all three cases, the harmonic scaling law for the state-to-state transition rates as a function of the vibrational quantum number was not respected. It was shown that this is due to the strong coupling of the different modes and the numerous adsorption sites. Including all dissipation channels the lifetimes followed a more regular behavior.

To evaluate the effect of the different dissipation models described above on state-resolved nuclear dynamics, we performed numerical simulations of the laser-driven selective subsurface absorption of hydrogen in a palladium (111) surface using laser distillation. Some small effects were found on a short time scale, the longer lifetimes of the surface states in the jellium model compared to the two other embedding densities allowing for a better excitation of an intermediate state which is subsequently decaying in the subsurface selectively. Repeating the excitation-relaxation sequence for performing laser distillation proved as efficient in the long run for all three embedding densities, although the longer-lived states of the jellium model converged more rapidly.

To summarize, only marginal differences for the lifetimes and the dynamics are found between the free metal and perturbed metal embedding-density models. Further, both models yield lifetimes which are in fair to good agreement with the model of Persson and co-workers for different reference geometries, contrary to the jellium model. However, the computation of the perturbed metal density is a tedious procedure involving many *ab initio* calculations and a fitting procedure that can become nontrivial for low sampling of complex environments. Further, the perturbation has to be computed for each type of atom, which renders the transition model presented above less transparent. On the other hand the free metal electronic density can be extracted for all positions of the adsorbate above and below the surface using a single periodic DFT calculation, and is valid for all atoms at once. Considering the small discrepancies between both models, we would strongly advocate using the latter for future applications, possibly in combination with the more flexible scaling factor in Eq. (13).

ACKNOWLEDGMENTS

This work was supported by the Sonderforschungbereich 450 of the Deutsche Forschungsgemeinschaft, *Analysis and Control of Ultrafast Photoinduced Processes* (subproject C7). Support by the European network on ''Electron Controlled Chemical Lithography'' (COST action CM0601) is also acknowledged.

*jean.c.tremblay@gmail.com

[1] U. Fano, Phys. Rev. **124**, 1866 (1961).
[2] D. C. Langreth, Phys. Rev. Lett. **54**, 126 (1985).
[3] D. Fuhrmann and C. Wöll, New J. Phys. **1**, 1 (1998).
[4] J. C. Tully, Annu. Rev. Phys. Chem. **51**, 153 (2000).
[5] A. R. P. Rau, Phys. Scr. **69**, C10 (2004).
[6] A. M. Wodtke, D. Matsiev, and D. J. Auerbach, Prog. Surf. Sci. **83**, 167 (2008).
[7] J. Kröger, J. Phys.: Condens. Matter **20**, 224015 (2008).
[8] J. Strömquist, L. Bengtsson, M. Persson, and B. Hammer, Surf. Sci. **397**, 382 (1998).
[9] A. C. Luntz, M. Persson, and G. O. Sitz, J. Chem. Phys. **124**, 091101 (2006).
[10] A. C. Luntz, M. Persson, S. Wagner, C. Frischkorn, and M. Wolf, J. Chem. Phys. **124**, 244702 (2006).
[11] J. I. Juaristi, M. Alducin, R. Díez Muiño, H. F. Busnengo, and A. Salin, Phys. Rev. Lett. **100**, 116102 (2008).
[12] M. Persson and B. Hellsing, Phys. Rev. Lett. **49**, 662 (1982).
[13] M. J. Puska and R. M. Nieminen, Phys. Rev. B **27**, 6121 (1983).
[14] B. Hellsing and M. Persson, Phys. Scr. **29**, 360 (1984).
[15] T. T. Rantala and A. Rosén, Phys. Rev. B **34**, 837 (1986).
[16] M. Head-Gordon and J. C. Tully, J. Chem. Phys. **96**, 3939 (1992).
[17] J. C. Tully, M. Gomez, and M. Head-Gordon, J. Vac. Sci. Technol. A **11**, 1914 (1993).
[18] N. Lorente and M. Persson, Faraday Discuss. **117**, 277 (2000).
[19] V. Krishna and J. C. Tully, J. Chem. Phys. **125**, 054706 (2006).
[20] H. Winter, J. I. Juaristi, I. Nagy, A. Arnau, and P. M. Echenique,

Phys. Rev. B **67**, 245401 (2003).
[21] N. Lorente and H. Ueba, Eur. Phys. J. D **35**, 341 (2005).
[22] S. Beyvers, Y. Ohtsuki, and P. Saalfrank, J. Chem. Phys. **124**, 234706 (2006).
[23] J. C. Tremblay and P. Saalfrank, J. Chem. Phys. **131**, 084716 (2009).
[24] A. C. Luntz, I. Makkonen, M. Persson, S. Holloway, D. M. Bird, and M. S. Mizielinski, Phys. Rev. Lett. **102**, 109601 (2009).
[25] P. Jena, F. Y. Fradin, and D. E. Ellis, Phys. Rev. B **20**, 3543 (1979).
[26] K. Blum, *Density Matrix Theory and Applications* (Plenum Press, New York, 1996).
[27] V. Gorini, A. Kossakowski, and E. C. G. Sudarshan, J. Math. Phys. **17**, 821 (1976).
[28] J. C. Tremblay, T. Klamroth, and P. Saalfrank, J. Chem. Phys. **129**, 084302 (2008).
[29] J. C. Tremblay, S. Beyvers, and P. Saalfrank, J. Chem. Phys. **128**, 194709 (2008).
[30] N. Ozawa, T. A. Roman, H. Nakanishi, H. Kasai, N. B. Arboleda, Jr., and W. A. Diño, J. Appl. Phys. **101**, 123530 (2007).
[31] J. T. Muckerman, Chem. Phys. Lett. **173**, 200 (1990).
[32] D. T. Colbert and W. H. Miller, J. Chem. Phys. **96**, 1982 (1992).
[33] R. W. Freund and N. M. Nachtigal, SIAM J. Sci. Comput. (USA) **15**, 313 (1994).
[34] J. C. Tremblay and T. Carrington, Jr., J. Chem. Phys. **125**, 094311 (2006).
[35] G. Kresse and J. Furthmuller, Phys. Rev. B **54**, 11169 (1996).
[36] G. Kresse and J. Furthmuller, Comput. Mater. Sci. **6**, 15 (1996).
[37] J. P. Perdew and Y. Wang, Phys. Rev. B **45**, 13244 (1992).
[38] H. J. Monkhorst and J. D. Pack, Phys. Rev. B **13**, 5188 (1976).
[39] M. Shirai, Y. Pu, M. Arai, and Y. Nishiyama, Appl. Surf. Sci. **126**, 99 (1998).
[40] M. Shirai and M. Arai, Langmuir **15**, 1577 (1999).
[41] S. K. Doyle, A. M. Shaikhudtinov, S. D. Jackson, and H.-J. Freund, Angew. Chem., Int. Ed. **42**, 5240 (2003).
[42] S. K. Doyle, A. M. Shaikhudtinov, and H.-J. Freund, J. Catal. **223**, 444 (2004).
[43] E. C. H. Sykes, L. C. Fernández-Torres, S. U. Nanayakkara, B. A. Mantooth, R. M. Nevin, and P. S. Weiss, Proc. Natl. Acad. Sci. U.S.A. **102**, 17907 (2005).
[44] J. Teschner, D. Borsodi, A. Wootsch, M. Révay, Z. Hävecker, A. Knop-Gericke, S. D. Jackson, and R. Schlögl, Science **320**, 86 (2008).
[45] W. Eberhardt, F. Greuter, and E. W. Plummer, Phys. Rev. Lett. **46**, 1085 (1981).
[46] O. M. Løwik and R. A. Olsen, Phys. Rev. B **58**, 10890 (1998).
[47] U. Muschiol, P. K. Schmidt, and K. Christmann, Surf. Sci. **395**, 182 (1998).
[48] G. K. Paramonov and P. Saalfrank, Chem. Phys. Lett. **301**, 509 (1999).
[49] M. Shapiro, E. Frishman, and P. Brumer, Phys. Rev. Lett. **84**, 1669 (2000).
[50] D. Gerbasi, M. Shapiro, and P. Brumer, J. Chem. Phys. **124**, 074315 (2006).